# Quantifying Multidimensional Effects of Physicochemical Parameters on PFAS Adsorption Using a Hybrid Response Surface Methodology-Machine Learning Approach

Harsh V. Patel[1], Jazmin Green[2], Hyo-Shin (John) Park[3], Stephanie Luster-Teasley Pass[1], Renzun Zhao[1,*]

[1]Department of Civil, Architectural, and Environmental Engineering, North Carolina A&T State University, Greensboro, NC 27411, USA

[2]Department of Computer Science, North Carolina A&T State University, Greensboro, NC 27411, USA

[3]Department of Engineering Management and Systems Engineering, Old Dominion University, Norfolk, VA 23529, USA

*Corresponding author. Phone: (336) 285-3684; fax: (336)-334-7540; e-mail: rzhao@ncat.edu

## Abstract

Per- and polyfluoroalkyl substances (PFAS) contamination has posed a significant environmental and public health challenge due to their ubiquitous nature. Adsorption has emerged as a promising remediation technique, yet optimizing adsorption efficiency remains complex due to the diverse physicochemical properties of PFAS and the wide range of adsorbent materials. Traditional modeling approaches, such as response surface methodology (RSM), struggled to capture nonlinear interactions, while standalone machine learning (ML) models required extensive datasets. This study addressed these limitations by developing hybrid RSM-ML models to improve the prediction and optimization of PFAS adsorption. A comprehensive dataset was constructed using experimental adsorption data, integrating key parameters such as pH, $pH_{pzc}$, surface area, temperature, and PFAS molecular properties. RSM was employed to model adsorption behavior, while gradient boosting (GB), random forest (RF), and extreme gradient boosting (XGB) were used to enhance predictive performance. Hybrid models—linear, RMSE-based, multiplicative, and meta-learning—were developed and evaluated. The meta-learning HOP-RSM-GB model achieved near-perfect accuracy ($R^2 = 1.00$, RMSE = 10.59), outperforming all other models. Surface plots revealed that low pH and high $pH_{pzc}$ maximized the adsorption while increasing log $K_{ow}$ consistently enhanced PFAS adsorption. These findings establish hybrid RSM-ML modeling as a powerful framework for optimizing PFAS remediation strategies. The integration of statistical and machine learning approaches significantly improves predictive accuracy, reduces experimental costs, and provides deeper insights into adsorption mechanisms. This study underscores the importance of data-driven approaches in environmental engineering and highlights future opportunities for integrating ML-driven modeling with experimental adsorption research.

## Keywords

Per- and Polyfluoroalkyl Substance (PFAS), Machine Learning, Response Surface Methodology, Adsorption, Distribution Coefficient.

## 1. Introduction

Per- and polyfluoroalkyl substances (PFAS) are synthetic chemicals used extensively in industrial applications and consumer products due to their chemical stability, thermal resistance, and water- and oil-repellent properties. Commonly found in nonstick cookware, firefighting foams, and water-resistant fabrics, PFAS has become pervasive in the environment, with contamination detected in soil, air, and particularly water systems (McNamara et al., 2018; Pramanik et al., 2015; Ross et al., 2018; Rostvall et al., 2018; D. Zhang et al., 2016a). These "forever chemicals" are characterized by their resistance to degradation under natural conditions, leading to their persistence in ecosystems and accumulation in biological organisms. The health impacts of PFAS exposure have been widely documented, including links to immune suppression, hormonal disruption, developmental delays in children, and increased risks of cancers. As of 2024, the U.S. Environmental Protection Agency (EPA) has established stringent Maximum Contamination Levels (MCLs) for perfluorooctanoic acid (PFOA), perfluorooctane sulfonic acid (PFOS), perfluorohexane sulfonic acid (PFHxS), perfluorononanoic acid (PFNA), and hexafluoropropylene oxide (HFPO) dimer acid as 4, 4, 10, 10, and 10 ng/L, respectively (US EPA, 2024). These limits underscore the urgency of developing effective remediation strategies to protect public health and comply with regulatory standards.

Among remediation techniques, adsorption has emerged as a promising approach due to its cost-effectiveness, scalability, and ability to target a wide range of PFAS compounds (Ross et al., 2018). Adsorption involves the transfer of PFAS molecules from the aqueous phase to the surface of a solid adsorbent, effectively reducing their concentration in contaminated water. Various materials, including activated carbon, biochar, ion-exchange resins, and mineral-based sorbents, have been explored as potential adsorbents. The efficiency of adsorption processes depends on several factors, including the physicochemical properties of the adsorbent and PFAS molecules, as well as operational conditions such as pH, temperature, and adsorbent dose.

Optimizing adsorption performance is a complex task due to the interplay of these variables and the diversity of PFAS compounds, which vary in molecular weight, chain length, hydrophobicity, and functional groups. Traditional experimental approaches, such as one-factor-at-a-time (OFAT) studies, are insufficient for capturing multidimensional interactions between variables and require extensive time and resources. To overcome these challenges, advanced statistical and computational methods are essential for systematically modeling and optimizing adsorption systems.

Response surface methodology (RSM) is a powerful statistical tool that systematically explores variable interactions and optimizes processes with fewer experiments (Abraham & Walsh, 1992; Burg et al., 2003; Kamlet et al., 1985; Sinha et al., 2022; Sprunger et al., 2007; K. Zhang et al.,

2020). In PFAS studies, RSM has been used to optimize degradation and adsorption processes, including PFOS removal via heterogeneous photocatalysis (83% removal in 8 hours) (de S. Furtado et al., 2021), PFOA adsorption using alginate hydrogel (94.8 ± 2.1% removal) (Naim Shaikh & Nawaz, 2024), and PFOA removal with layered double hydroxides and peroxydisulfate activation (H. Yang et al., 2022). These investigations demonstrate RSM's effectiveness in optimizing operational parameters and adsorbent design for PFAS treatment under mild conditions. However, its reliance on polynomial regression can limit capturing complex nonlinear and higher-order interactions, suggesting the need for complementary approaches when dealing with diverse PFAS compounds and adsorbents.

Machine learning (ML) offers advanced capabilities for modeling complex adsorption processes by uncovering nonlinear relationships, variable interactions, and hidden patterns without relying on predefined equations. Popular algorithms such as random forest (RF), gradient boosting (GB), and extreme gradient boosting (XGB) show high predictive accuracy and can rank the influence of parameters (e.g., pH, hydrophobicity) on adsorption outcomes (Karbassiyazdi *et al.*, 2022a). However, large and diverse datasets are essential for accurate training an ML model, which can be resource-intensive in PFAS research. Integrating response surface methodology (RSM) with ML in hybrid models addresses this challenge: RSM generates structured datasets and identifies key variables, while ML enhances predictive performance by capturing nonlinearities and higher-order interactions. Although hybrid models have been successfully applied to areas like wastewater treatment and heavy metal adsorption, their use in PFAS adsorption remains limited, highlighting a promising avenue for future research.

In PFAS adsorption studies, hybrid RSM-ML models can: (1) accurately predict $K_d$ across a wide range of adsorbents and conditions, (2) identify the most influential factors driving adsorption performance, (3) optimize process parameters to maximize PFAS distribution, and (4) reduce the need for exhaustive experimentation, saving time and resources.

This study aims to develop a comprehensive RSM-ML framework for modeling and optimizing the adsorption of PFAS on various adsorbent materials. The specific objectives are to: Investigate the effects of adsorbent properties, PFAS characteristics, and process conditions on the distribution coefficient ($K_d$) using RSM; Implement and compare hybrid RSM-ML algorithms, including RF, GB, and XGB, to predict $K_d$ and evaluate their performance relative to RSM; Develop hybrid models to enhance predictive accuracy and capture complex variable interactions; and Optimize process parameters to maximize PFAS distribution coefficient and provide insights into variable significance for guiding future research and development.

## 2. Methodology

### 2.1 Data Mining

To construct a comprehensive dataset for modeling PFAS adsorption, we integrated experimental data mining from literature with synthetic data generation derived from isotherm equations. This approach facilitated the development of a robust dataset encompassing distribution coefficients ($K_d$) and key physicochemical variables essential for understanding adsorption processes. The

primary source of data was peer-reviewed literature reporting adsorption experiments for PFAS. These studies included experimental details such as adsorption isotherms, BET surface area, and equilibrium concentration ranges ($C_e$). Adsorption isotherms, including widely used models such as the Freundlich equation ($Q_e = K_f * C_e^{1/n}$), provided the foundation for deriving additional data points. From the literature, isotherm parameters ($K_f$, 1/n) were extracted through regression fitting of experimental data. Using the established isotherm equations, equilibrium concentrations ($C_e$) spanning the reported range in each study were substituted to calculate corresponding $Q_e$ values, representing the amount of PFAS adsorbed per unit mass of absorbent. The calculated $Q_e$ values were then used to determine the distribution coefficient ($K_d$), a critical parameter reflecting the equilibrium partitioning of PFAS between the solid and liquid phases ($K_d = Q_e/C_e$). This process was repeated systematically to generate synthetic data, ensuring that each isotherm contributed at least 15 data points within its experimental range. This interpolation strategy enriched the dataset while maintaining consistency with the original experimental framework. Table S1 lists studies from which the data was mined for $K_d$. 2580 data points were collected from 172 isotherms obtained from more than 30 journal articles published on 73 unique adsorbents and 10 PFAS compounds (PFOS, PFOA, PFHxS, PFHxA, PFBS, PFBA, Gen-X, PFHpA, PFDA, and PFDoDA) between 2009 and 2025 (Ateia et al., 2018; Campos-Pereira et al., 2020; Chang et al., 2019, 2020; W. Chen et al., 2017; X. Chen et al., 2011a, 2011b; Deng et al., 2012; Fagbayigbo et al., 2017; Jian et al., 2019; Lei, Lian, et al., 2022; Lei, Yao, et al., 2022; L. Liu et al., 2018; T. Liu et al., 2018; Meng et al., 2019; Patel et al., 2025; Qian et al., 2017; Senevirathna et al., 2010; Tang et al., 2010; B. Wang et al., 2016; F. Wang et al., 2012; F. Wang & Shih, 2011; Xing et al., 2020; A. Yang et al., 2020; Yoon et al., 2025; Yu et al., 2009; D. Zhang et al., 2016b; Q. Zhang et al., 2011; Zhao et al., 2014; Zhi & Liu, 2016; Zhou et al., 2010).

In parallel, the physicochemical properties of PFAS and adsorbent materials were also mined from the literature. BET surface area ($m^2/g$) data were directly extracted, providing insights into the adsorbent's structural properties. Additional PFAS molecular properties, including Abraham solvation parameters (A, B, S, E, V), were computed using the ACD/Labs Percepta platform. These parameters quantify molecular interactions, such as hydrogen bonding (A, B), polarity/polarizability (S, E), and molecular size/volume (V), offering a detailed understanding of PFAS behavior during adsorption. This comprehensive methodology ensured that the dataset captured critical variables influencing adsorption processes. By combining experimental isotherm data with computational descriptors, this study bridges empirical insights and theoretical modeling. The resulting dataset supports advanced computational techniques, such as response surface methodology (RSM) and machine learning (ML), for predicting and optimizing PFAS adsorption across diverse adsorbent materials and environmental conditions.

## 2.2 Response Surface Methodology (RSM) Framework

The response surface methodology (RSM) was employed as a systematic and statistical approach to model the distribution coefficient ($K_d$) for PFAS compounds on various adsorbents. RSM provides a structured framework for identifying the relationships between key independent variables and the response variable, $K_d$. The analysis was designed to quantify the linear, non-

linear effects, and interaction effects of the independent variables, enabling a comprehensive exploration of the multivariable space.

Quadratic and higher-order polynomial (HOP) regression was used for RSM. The independent variables included pH, adsorbent dose (g/L), temperature (°C), initial concentration ($C_0$, mg/L), BET surface area ($m^2/g$), and physicochemical properties of PFAS compounds such as $pK_a$, log $K_{ow}$, molecular weight (mg/mmol), and Abraham solvation parameters (A, B, S, E, V). These variables were selected based on their relevance to adsorption mechanisms and their established influence on PFAS adsorption.

The response variable, $K_d$, was derived from the relationship $K_d = Q_e/C_e$, where $Q_e$ represents the equilibrium adsorption capacity, and $C_e$ is the equilibrium concentration of PFAS in the solution. Experimental data from the literature and synthetic data generated from isotherm models were used to populate the data matrix. The quadratic and higher-order polynomial regression RSM models are given as equations (1) and (2).

$$K_d = \beta_0 \sum_{i=1}^{k} \beta_i X_i + \sum_{i=1}^{k} \beta_{ii} X_i^2 + \sum_{i=1}^{k} \sum_{j=i+1}^{k} \beta_{ij} X_i X_j + \epsilon \quad (1)$$

$$K_d = \beta_0 + \sum_{i=1}^{n} \beta_i X_i + \sum_{i=1}^{n} \beta_{ii} X_i^2 + \sum_{i<j} \beta_{ij} X_i X_j + \sum_{i=1}^{n} \beta_{iii} X_i^3 + \sum_{i<j<k} \beta_{ijk} X_i X_j X_k + \epsilon \quad (2)$$

where $\beta_0$ is the intercept, $\beta_i$, $\beta_{ii}$, $\beta_{ij}$, $\beta_{iii}$, and $\beta_{ijk}$ are the regression coefficients for linear, quadratic, and interaction terms, respectively, $X_i$, $X_j$, and $X_k$ are the independent variables, and $\epsilon$ is the residual error. The adequacy of the model and significance of each linear, non-linear, and interactive term based on independent variables was assessed through analysis of variance (ANOVA), and coefficient of determination ($R^2$).

### 2.3 Machine Learning (ML) Models

To complement the RSM framework and address its limitations in capturing nonlinear and high-order interactions, machine learning (ML) algorithms were employed. The ML models used in this study included random forest (RF), gradient boosting (GB), and extreme gradient boosting (XGB), which have demonstrated strong performance in modeling complex environmental processes. These models were trained to predict $K_d$ based on the same independent variables used in the RSM analysis. RF is an ensemble learning method that constructs multiple decision trees during training and averages their predictions to enhance accuracy and reduce overfitting. The algorithm's ability to handle multicollinearity and nonlinear relationships makes it particularly suitable for adsorption studies. GB builds sequential decision trees, with each tree correcting the errors of its predecessor. This iterative approach enables the model to achieve high predictive accuracy and uncover intricate relationships within the dataset. XGB, an optimized implementation of gradient boosting, incorporates advanced features such as regularization to prevent overfitting and parallel processing to improve computational efficiency. These characteristics make XGB a powerful tool for high-dimensional adsorption datasets.

Each ML model was trained on 80% of the dataset and validated on the remaining 20% using k-fold cross-validation (k = 5) to ensure robustness and minimize overfitting. The performance of

the models was evaluated using key metrics, including the coefficient of determination ($R^2$), root mean square error (RMSE), mean absolute error (MAE), and mean square error (MSE).

### 2.4 Hybrid RSM-ML Models

In this study for hybrid modeling, QRSM and HOP-RSM were combined with RF, GB, and XGB models to optimize adsorption parameters and predict distribution coefficients ($K_d$). QRSM incorporates linear, squared, and interaction terms to model adsorption behavior. At the same time, HOP-RSM extends this framework with higher-degree polynomial terms, allowing for improved precision in capturing more intricate adsorption interactions.

Several hybrid RSM-ML frameworks were employed to improve predictive accuracy:

1. Linear Hybrid Model (LHM): This method corrects RSM predictions using ML-based residual adjustments, enhancing accuracy without sacrificing interpretability. However, it may struggle with highly nonlinear interactions that cannot be captured by simple residual corrections.

2. RMSE-Based Dynamic Hybrid Model: This approach dynamically selects either the RSM or ML component based on Root Mean Square Error (RMSE) performance, ensuring optimal prediction for varying adsorption conditions. However, it requires computationally intensive cross-validation to determine the best model at each instance.

3. Multiplicative Hybrid Model: Instead of additive polynomial terms, this model introduces multiplicative interactions between adsorption parameters, which helps in modeling synergistic and antagonistic adsorption effects. However, it has a more complex parameter space, making optimization challenging.

4. Metal Model Hybridization: This ensemble-based approach combines multiple ML models (e.g., GB, XGBoost, Random Forests) with RSM to improve robustness and reduce overfitting. While it provides high predictive accuracy, it comes with increased computational cost and complexity in hyperparameter tuning.

#### 2.4.1 Model Performance

The predictive accuracy and generalizability of the models were validated using the 20% test dataset. For hybrid models, the performance was compared against stand-alone RSM and ML models to assess their ability to capture complex variable interactions and improve prediction accuracy. Statistical parameters such as R-squared, RSME, MSE, and MAE were used to compare the prediction accuracy of each model.

#### 2.4.2 Surface plots

Based on the significance determined from ANOVA analysis, surface plots were generated for the most significant pair of descriptors for $K_d$. Surface plots were used to visualize the linear, non-linear, and interactive effects of the descriptor pair on $K_d$.

#### 2.4.1 Feature Importance Analysis

Feature importance analysis was performed for the ML and hybrid models to quantify the relative contribution of each independent variable to the prediction of $K_d$. For ensemble models such as RF, GB, and XGB, the feature importance scores were derived from the mean decrease in impurity (Gini index) or gain, depending on the algorithm. These scores provided valuable insights into the factors most strongly influencing PFAS adsorption, guiding the development of targeted remediation strategies. Results for feature importance are showcased in SI with Figure S6, S7, and S8.

## 3 Results and Discussion

### 3.1 Response Surface Methodology

The response surface methodology (RSM) model using quadratic and higher-order polynomial (HOP) regression provided a detailed understanding of the relationships between key variables and the distribution coefficient ($K_d$) for PFAS adsorption. The HOP regression model captured linear, non-linear, and interaction effects of the variables, including surface area, $pH_{pzc}$, molecular weight, $pK_a$, pH, temperature, log $K_{ow}$, adsorbent dose, initial concentration, and Abraham solvation parameters (A, B, S, E, V). The regression coefficients, standard errors (SE), t-statistics, and p-values were calculated to evaluate the significance and statistical soundness of each linear, non-linear, and interactive term. However, the significance level of these linear, non-linear, and interactive terms was found to be different, as shown in Table 1 and Table S2. Table 1 presents the results of a Higher-Order Polynomial Response Surface Methodology (HOP-RSM) regression model, which estimates the influence of various physicochemical parameters on the distribution coefficient ($K_d$). The coefficients (Estimate) represent the magnitude and direction of each parameter's effect on $K_d$, while the standard error (SE), t-statistic (t-Stat), and p-value (p-value) provide insight into the statistical significance of each predictor.

Among the linear terms, the Surface Area (1.366, $p = 0.002$) shows a positive and statistically significant effect on $K_d$, suggesting that a larger surface area enhances adsorption capacity. Similarly, $pH_{pzc}$ (302.180, $p = 0.031$) has a positive effect, indicating that materials with a higher point of zero charge ($pH_{pzc}$) tend to favor PFAS adsorption, likely due to stronger electrostatic interactions. $pK_a$ (14.909, $p = 0.040$) also exhibits a positive and significant influence, implying that the acid dissociation constant of PFAS compounds plays a key role in their adsorption behavior. The pH (-1315.724, $p = 0.022$) term is negative, indicating that increasing pH reduces $K_d$, which aligns with expectations since higher pH values can increase electrostatic repulsion between PFAS and the adsorbent surface.

Temperature (403.035, $p = 0.041$) has a significant positive effect, implying that higher temperatures might enhance adsorption by increasing diffusion rates or favoring specific adsorption mechanisms. Log $K_{ow}$ (18.133, $p = 0.007$) also has a significant impact, confirming that hydrophobic interactions play a role in PFAS adsorption. However, molecular weight (56.610, $p = 0.891$) is not statistically significant, suggesting that molecular size alone does not strongly influence $K_d$ within the studied range. Besides molecular weight, the other non-significant terms are given in Table S2 with detailed explanations in supporting information.

One limitation of this HOP-RSM model is that it only considers linear relationships between the predictors and $K_d$. The absence of non-linear and interaction terms means that the model does not account for complex adsorption behaviors, such as synergistic or antagonistic effects between variables. For example, adsorption processes often involve non-linear dependencies on pH and $pK_a$, yet these effects are not captured in the current model. Additionally, the large standard error for some parameters (e.g., $pK_a$: 3224.192) suggests possible overfitting or collinearity among predictors, which could impact the reliability of the estimates.

Overall, while the model provides valuable insights into the primary factors influencing PFAS adsorption, further analysis incorporating machine learning model to capture non-linearity would improve predictive accuracy and better describe adsorption mechanisms.

Table 1: Estimated coefficients for *significant* parameters obtained from *the HOP – RSM model*. (NaN: Not A Number)

| Row | Estimate | SE | t-Stat | p-value |
|---|---|---|---|---|
| **(Intercept)** | 0.000 | 0.000 | | |
| **Surface Area** | 1.366 | 0.442 | 3.089 | 0.002 |
| **$pH_{pzc}$** | 302.180 | 295.267 | 2.023 | 0.031 |
| **Molecular weight** | 56.610 | 411.968 | 0.137 | 0.891 |
| **$pK_a$** | 14.909 | 3224.192 | 3.005 | 0.040 |
| **pH** | -1315.724 | 1081.786 | -2.216 | 0.022 |
| **Temperature** | 403.035 | 197.319 | 2.043 | 0.041 |
| **Log $K_{ow}$** | 18.133 | 1087.640 | 2.017 | 0.007 |

## 3.2 Model Performance

The predicted versus actual $K_d$ plot compared six modeling approaches: HOP-RSM, GB, Linear HOP-RSM-GB, RMSE-based HOP-RSM-GB, Multiplicative HOP-RSM-GB, and Meta HOP-RSM-GB shown in Figure 1 and data for the models is given on Table S3. The distribution of points around the ideal y = x line revealed distinct differences in predictive accuracy among these models. The meta-model (Meta HOP-RSM-GB) exhibited the highest alignment with the ideal line, achieving an $R^2$ of 1.00, RMSE of 10.59, MSE of 112.21, and MAE of 3.95. This indicated near-perfect predictive performance due to the ensemble's ability to capture both

global trends and local variations in adsorption behavior.

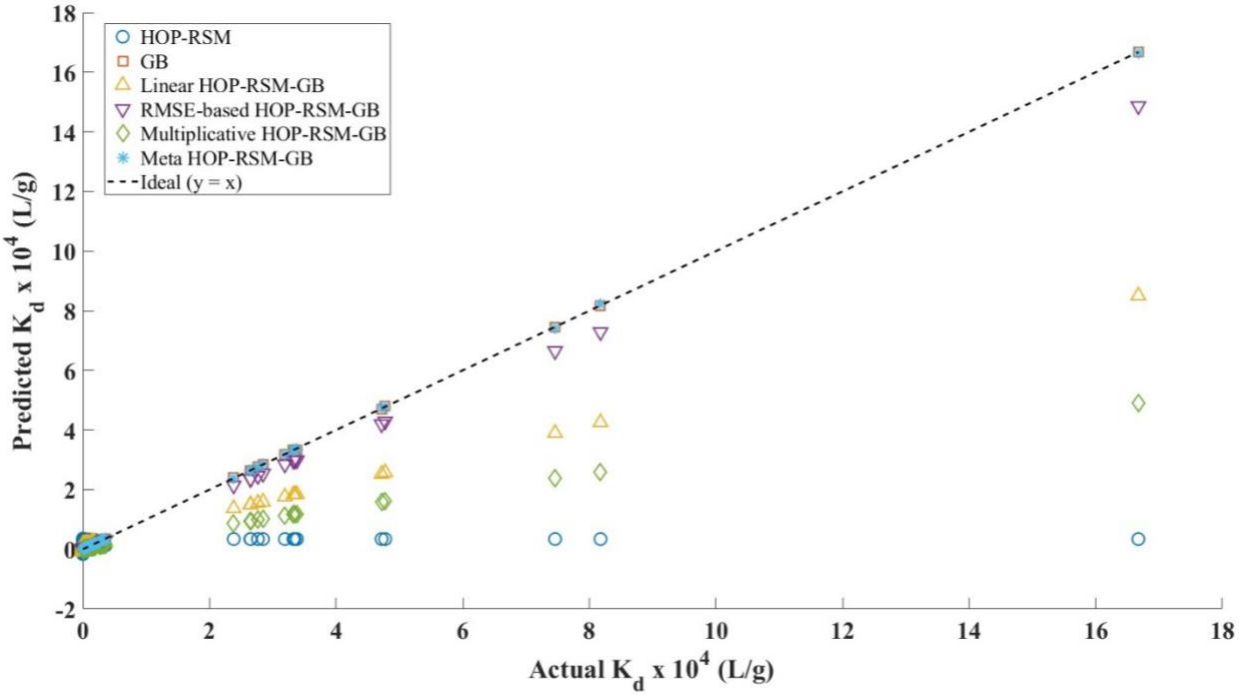


Figure 1: Predicted vs Actual $K_d$ scatter plot to compare the performance of stand-alone and hybrid HOP-RSM-GB models.

The RMSE-based hybrid (RMSE-based HOP-RSM-GB) also demonstrated strong predictive accuracy, with an $R^2$ of 0.99, RMSE of 488.82, MSE of 238940.5, and MAE of 52.84. While slightly less accurate than the meta-model, this approach significantly improved over the individual models by optimizing parameter selection through RMSE minimization. The stand-alone gradient boosting model (GB) performed well, with an $R^2$ of 1.00, RMSE of 50.12, MSE of 2511.66, and MAE of 22.81, indicating that GB effectively captured nonlinearity but lacked the refinement introduced by hybridization with polynomial regression.

Conversely, the linear hybrid model (Linear HOP-RSM-GB) exhibited lower predictive accuracy, with an $R^2$ of 0.75, RMSE of 2421.87, MSE of 5856464.17, and MAE of 397.61. Its larger deviations from the ideal line were particularly pronounced at higher $K_d$ values, suggesting limitations in capturing complex nonlinear interactions between process conditions and adsorption. The multiplicative hybrid (Multiplicative HOP-RSM-GB) performed similarly, with an $R^2$ of 0.53, RMSE of 3106.61, MSE of 9651020.85, and MAE of 205.43, indicating moderate improvement over pure polynomial regression but an inability to fully capture adsorption dynamics.

The HOP-RSM model exhibited the weakest performance, with an $R^2$ of 0.04, RMSE of 4410.14, MSE of 19449354.35, and MAE of 830.48. The severe underestimation of higher $K_d$ values and broad scatter indicated the model's failure to generalize beyond lower adsorption capacities, a limitation stemming from polynomial regression's sensitivity to multicollinearity and overfitting in high-dimensional feature spaces. The disparities in model performance

suggested that standalone polynomial regression models lacked the flexibility to model nonlinear adsorption behaviors accurately, while hybridization with GB, particularly through RMSE-based and meta-learning approaches, significantly improved predictive accuracy by leveraging the strengths of both regression-based and tree-based methodologies.

The hybrid HOP-RSM with GB model had the highest predictive accuracy and least error values compared to stand-alone models, hybrid QRSM models, and hybrid HOP-RSM with RF and XGB models as shown in Table S3. The predicted vs actual $K_d$ plots for the other 5 hybrid models are shown in Figures S1, S2, S3, S4, and S5.

### 3.3 Interactive Surface Plots

Based on the t-stat and p-value the significant parameters were selected for surface plots to visualize the interactive effect of these parameters on $K_d$. Figure 2 illustrates the interactive effects of surface area ($m^2/g$) and $pH_{pzc}$ on the distribution coefficient ($K_d$) for PFAS adsorption. The surface exhibits a curved profile, highlighting the nonlinear relationship between these variables. Adsorbents with surface areas in the range of 1,000 – 2,000 $m^2/g$ demonstrate increased $K_d$, when the $pH_{pzc}$ is in the range of 6 – 10, indicating enhanced adsorption performance due to the greater availability of active binding sites. Similarly, $pH_{pzc}$ plays a significant role, where $K_d$ increases with $pH_{pzc}$ until it reaches 10. When $pH_{pzc}$ was higher than 10, $K_d$ values showed a decreasing pattern. This trend reflects the ability of adsorbents with higher $pH_{pzc}$ to maintain a positively charged surface, favoring interactions with negatively charged PFAS molecules. However, at very high surface areas or extreme $pH_{pzc}$ values, the adsorption performance plateaus suggest potential saturation effects. The plot underscores the importance of optimizing both adsorbent surface area and surface charge properties to maximize PFAS removal efficiency under various environmental conditions.

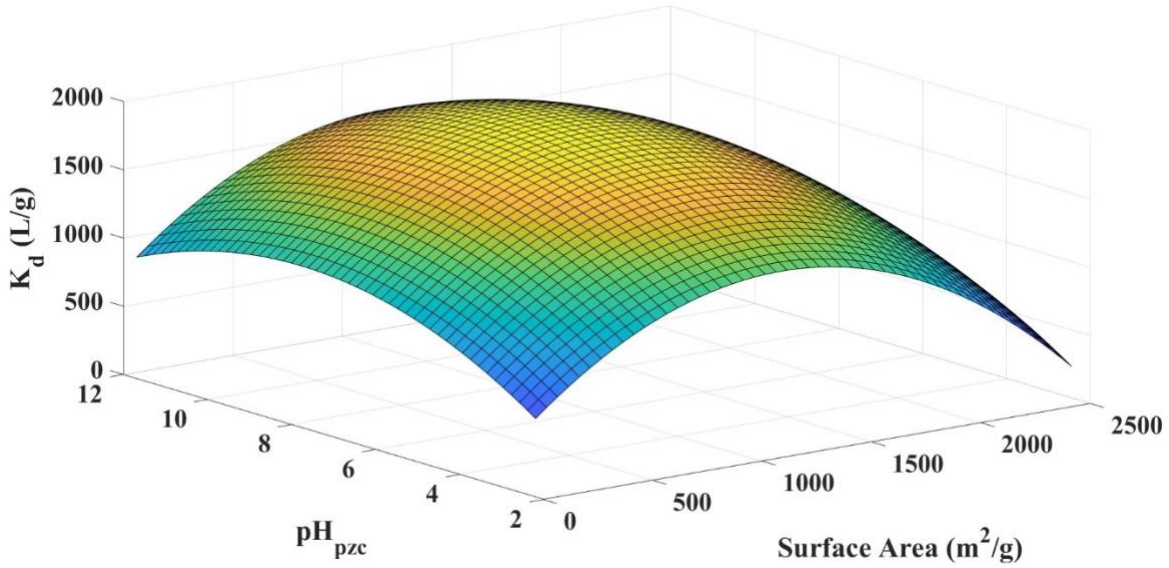


Figure 2: Response Surface plot showing the interactive effect of surface area and $pH_{pzc}$ on $K_d$.

The surface plot in Figure 3 illustrates the relationship between the distribution coefficient ($K_d$, L/g) and two key predictor variables: Surface Area ($m^2/g$) and $pK_a$ using the HOP-RSM XGB meta-model. The surface shows that $K_d$ reaches its peak at moderate surface areas (~1000–1500 $m^2/g$) and higher $pK_a$ values (~0 to 4). This suggests that adsorption efficiency is highest when the adsorbate has a moderate to high $pK_a$, allowing better interaction with the adsorbent surface. However, beyond ~1500 $m^2/g$, $K_d$ declines, likely due to pore blockage, diffusion limitations, or reduced availability of active sites, indicating that excessive surface area does not always enhance adsorption.

The effect of $pK_a$ on $K_d$ is also significant. At low $pK_a$ values (~ -4 to 0), Kd remains low, suggesting weaker adsorption due to the adsorbate being in a highly ionized state. As $pK_a$ increases, $K_a$ rises, indicating stronger hydrophobic or π–π interactions. The curvature of the surface plot highlights the interactive effect of surface area and $pK_a$, suggesting that adsorption efficiency depends on achieving an optimal balance between these two factors. Simply increasing surface area does not guarantee higher adsorption, emphasizing the need to optimize both adsorbent properties and chemical interactions for effective contaminant removal.

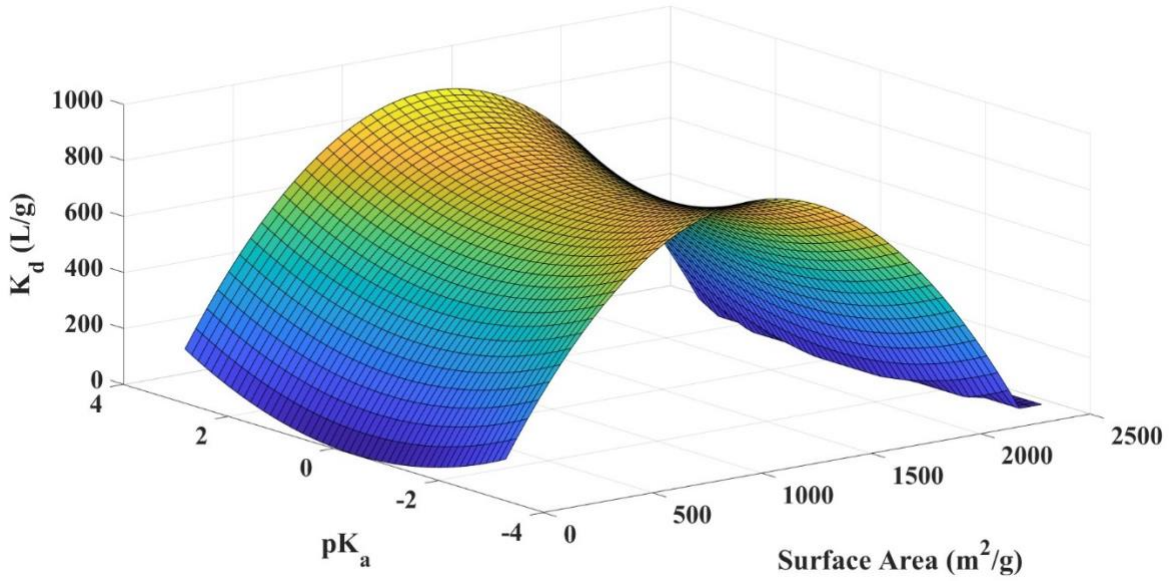


Figure 3: Surface plot showing the interactive effect of $pK_a$ and surface area on $K_d$.

Figure 4 depicts the relationship between the distribution coefficient ($K_d$, L/g) and two key variables: Surface Area ($m^2/g$) and Temperature (°C), modeled using a HOP-RSM XGB meta-model. The plot demonstrates a parabolic trend, where $K_d$ increases with surface area and temperature up to a certain threshold before gradually decreasing. This indicates that both factors

contribute significantly to adsorption efficiency, but their effects are nonlinear.

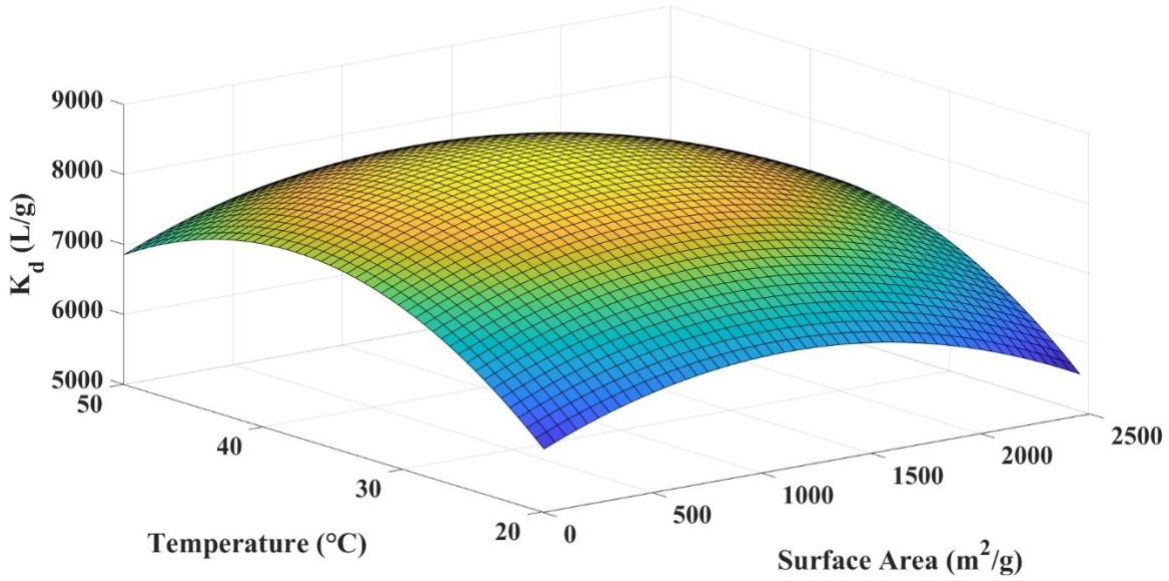


Figure 4: Surface plot showing the interactive effect of temperature and surface area on $K_d$.

At moderate surface area (~1000–1500 m²/g) and temperature (~30–40°C), $K_d$ reaches its maximum, suggesting that an optimal combination of surface properties and thermal conditions enhances adsorption. However, beyond ~1500 m²/g surface area and above ~40°C, adsorption efficiency declines, likely due to desorption effects, decreased adsorbate-adsorbent interactions, or structural changes in the adsorbent material. The surface plot highlights the interactive nature of surface area and temperature, reinforcing that excessively high temperatures may weaken adsorption forces, while extreme surface area values may not always improve adsorption due to diffusion limitations or reduced active site accessibility.

The surface plot in Figure 5 illustrates the relationship between the distribution coefficient ($K_d$, L/g) and two key chemical parameters: $pK_a$ and pH at the point of zero charge ($pH_{pzc}$). Generated using a HOP-RSM XGB meta-model, the plot highlights the interactive effects of these parameters on adsorption efficiency. The surface exhibits a nonlinear curvature, indicating that $K_d$ is maximized at moderate $pK_a$ (~0 to 2) and $pH_{pzc}$ values (~6 to 8), suggesting optimal adsorption conditions when the adsorbate has moderate ionization potential, and the adsorbent surface charge is near neutrality.

At low $pK_a$ values (~ -4 to 0), $K_d$ remains low, likely due to the adsorbate being predominantly ionized, which weakens its interaction with the adsorbent. Similarly, at extreme $pH_{pzc}$ values (~2 or ~10–12), $K_d$ declines, possibly due to strong repulsive forces between the adsorbate and adsorbent surface. The wave-like curvature of the surface plot emphasizes the complex interplay between electrostatic interactions and hydrophobic adsorption mechanisms, reinforcing the importance of balancing adsorbate chemistry ($pK_a$) and adsorbent surface charge ($pH_{pzc}$) for

maximizing adsorption performance.

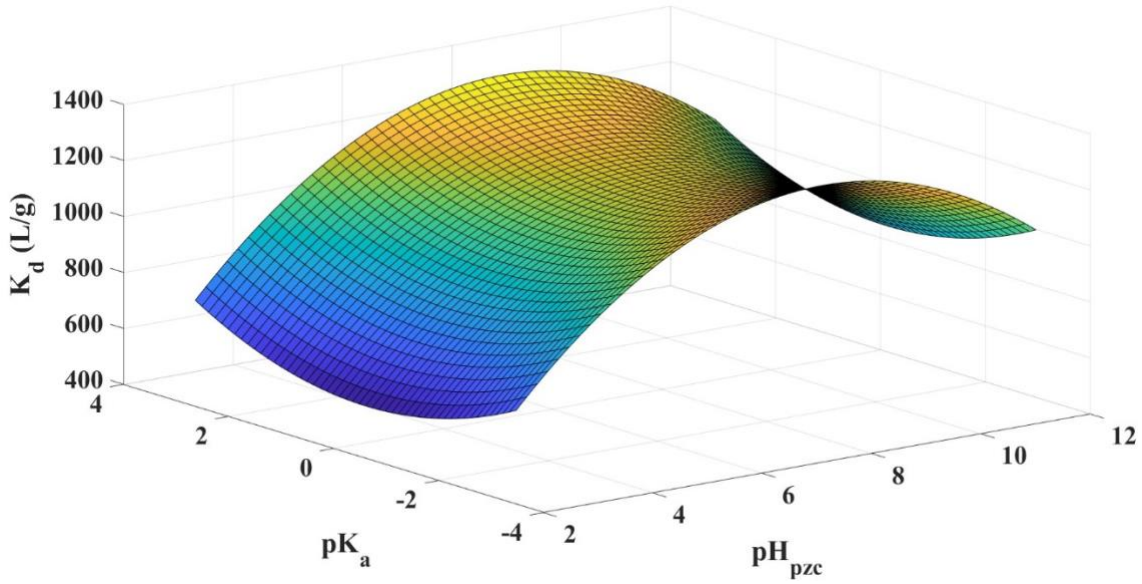


Figure 5: Surface plot showing the interactive effect of $pK_a$ and $pH_{pzc}$ on $K_d$.

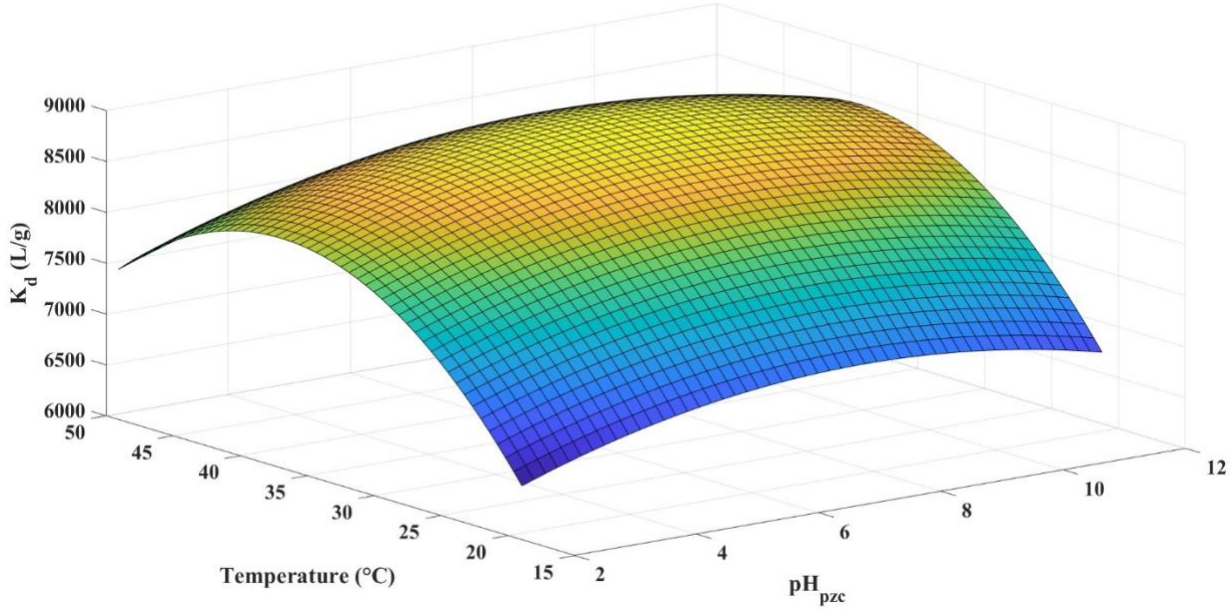


Figure 6: Response Surface plot showing the combined effect of $pH_{pzc}$ and temperature on $K_d$.

Figure 6 illustrates the interaction between $pH_{pzc}$ and temperature (°C) on the distribution coefficient ($K_d$) for PFAS adsorption. The surface displays a nonlinear curvature, indicating that both variables significantly influence adsorption performance. Temperature has a positive effect on $K_d$, with moderate increases in temperature promoting adsorption, possibly due to enhanced molecular interactions and increased kinetic energy facilitating PFAS diffusion to adsorption sites. However, the plot also reveals a saturation effect, where the influence of temperature and

$pH_{pzc}$ plateaus at higher values, suggesting that further increases in these parameters do not yield proportional improvements in adsorption efficiency. The interaction between temperature and $pH_{pzc}$ suggests optimal adsorption conditions at moderate temperature levels (around 30 – 35 °C) and higher $pH_{pzc}$ values. These insights highlight the need for balancing operational parameters to maximize PFAS removal efficiency under practical environmental conditions.

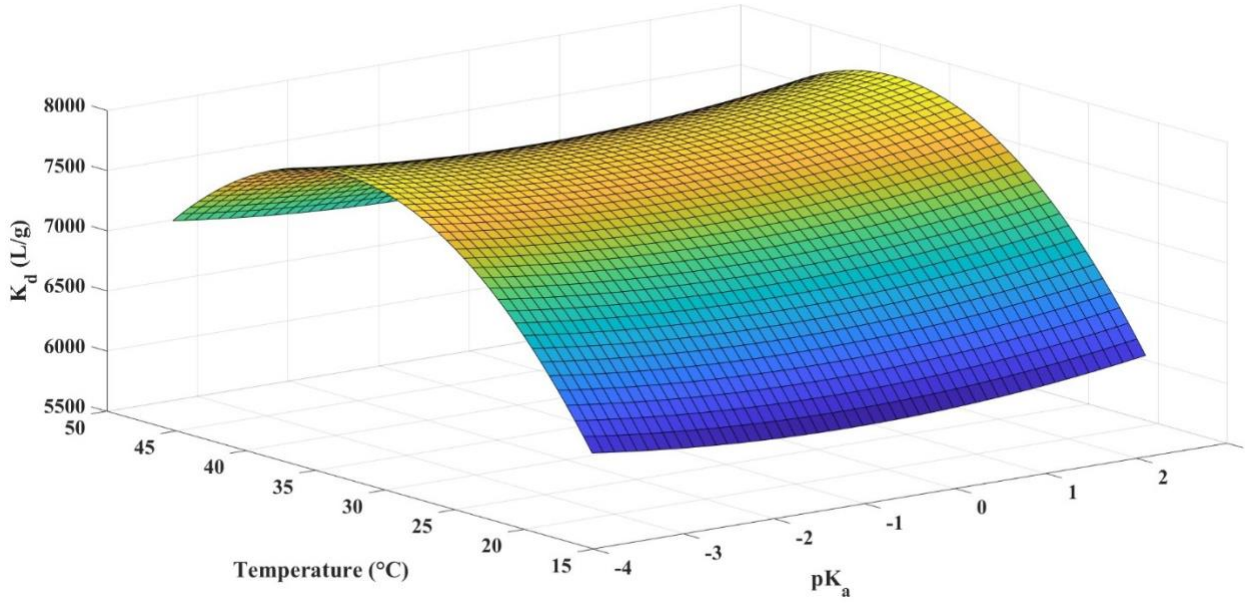


Figure 7: Response Surface plot showing the combined effect of $pK_a$ and temperature on $K_d$.

Figure 7 illustrates the combined effects of $pK_a$ and temperature (°C) on the distribution coefficient ($K_d$) for PFAS adsorption. The surface demonstrates a nonlinear interaction between the variables, with both temperature and $pK_a$ significantly influencing adsorption performance. As $pK_a$ increases toward neutral or slightly acidic values, $K_d$ also increases, indicating that PFAS compounds with higher $pK_a$ exhibit better adsorption under certain conditions. This may be attributed to enhanced molecular interactions or ionization effects that improve binding to the adsorbent surface.

Similarly, higher temperatures positively affect $K_d$, suggesting that increased thermal energy facilitates PFAS diffusion and interaction with adsorption sites. The interaction between $pK_a$ and temperature is evident, as their combined influence creates regions of optimal adsorption efficiency. The highest $K_d$ values are observed at temperatures between 30 – 35 °C and moderate $pK_a$ values (near -1 to 1), indicating a synergistic relationship. Conversely, lower $pK_a$ values and lower temperatures result in reduced adsorption efficiency, as reflected in the lower $K_a$ values. This analysis highlights the importance of carefully optimizing both pKa-related conditions and operational temperatures to achieve maximum PFAS removal efficiency in adsorption processes.

While the RSM model captured some meaningful trends, its overall predictive performance was limited. The moderate $R^2$ value of 0.031924 suggests that the model explains a portion of the variability in $K_d$, but the high p-values for many terms indicate potential overfitting or insufficient data diversity. These limitations are likely due to multicollinearity among variables,

the inherently nonlinear nature of PFAS adsorption, and the relatively small dataset size. Despite these limitations, the RSM analysis provides practical insights into optimizing PFAS adsorption. The negative impact of pH highlights the importance of maintaining acidic conditions for effective adsorption, particularly for charged PFAS species. The positive effects of surface area and $pH_{pzc}$ emphasize the role of adsorbent design in achieving high $K_d$ values. These findings align with established principles of adsorption science and can guide the development of tailored remediation strategies.

Figure 8 illustrates the non-linear relationship between Log $K_{ow}$ and surface area, and its interactive effect on $K_d$. Low Log $K_{ow}$ resulted in low $K_d$ and high Log $K_{ow}$ resulted in high $K_d$, regardless of the surface area. These findings support the idea that PFAS compounds with higher hydrophobicity will have higher distribution coefficient and removal regardless of the adsorbent material.

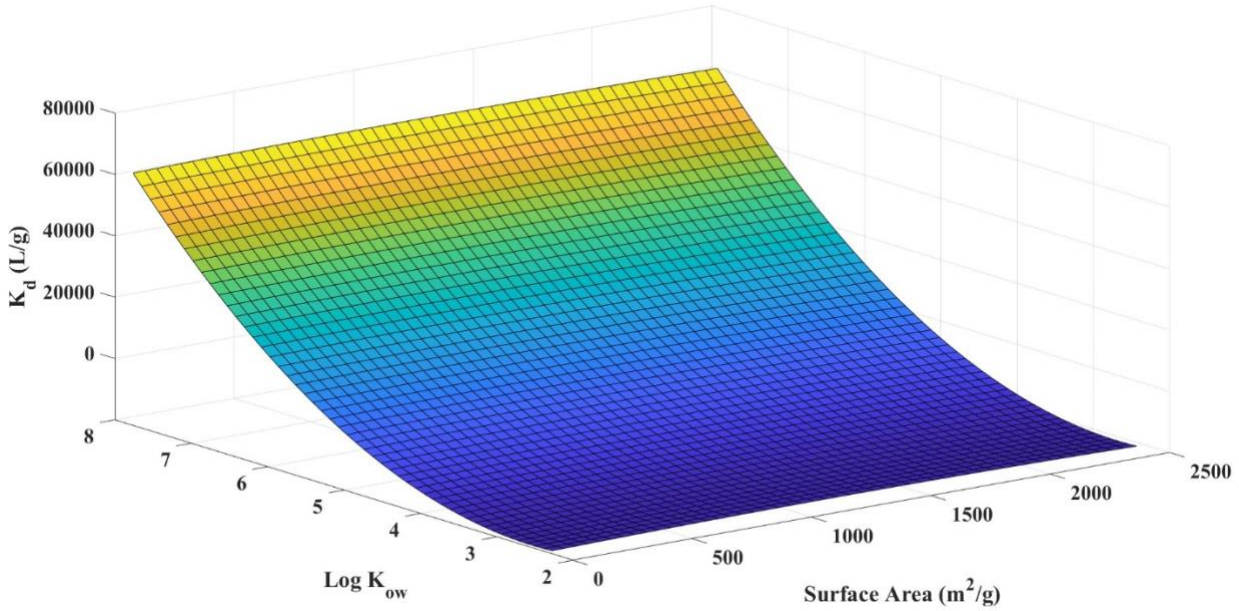


Figure 8: Response Surface plot showing the combined effect of Log $K_{ow}$ and surface area on $K_d$.

The surface plot in Figure 9 illustrates the relationship between the $K_d$, pH, and $pH_{pzc}$, providing insight into how electrostatic interactions influence PFAS adsorption. The quadratic response surface model (RSM) results indicate that both pH and $pH_{pzc}$ significantly impact adsorption, with regression coefficients of -1315.724 for pH and 302.180 for $pH_{pzc}$, and respective p-values of 0.022 and 0.031, confirming their statistical significance. The negative coefficient for pH suggests that increasing pH decreases $K_d$, which aligns with the expected electrostatic behavior of PFAS adsorption. At high pH, the adsorbent surface is negatively charged ($pH > pH_{pzc}$), leading to electrostatic repulsion with the anionic PFAS species, thereby reducing adsorption efficiency. Conversely, at low pH, the adsorbent surface carries a positive charge ($pH < pH_{pzc}$), promoting electrostatic attraction and enhancing PFAS adsorption. The positive coefficient for $pH_{pzc}$ indicates that materials with a higher $pH_{pzc}$ exhibit greater $K_d$, suggesting that high $pH_{pzc}$

materials are more effective for PFAS adsorption. A higher $pH_{pzc}$ value means the material retains a positive charge over a wider pH range, reinforcing electrostatic attraction with anionic PFAS.

The curvature of the surface plot demonstrates a strong interaction effect between pH and $pH_{pzc}$. At low pH and high $pH_{pzc}$, $K_d$ reaches its maximum, confirming that PFAS adsorption is optimized under conditions where the adsorbent remains positively charged. However, at high pH and low $pH_{pzc}$, $K_d$ becomes highly negative, suggesting a repulsion-dominated desorption mechanism. The nonlinear adsorption response further highlights the complex interplay between electrostatic interactions and potential hydrogen bonding at intermediate pH values.

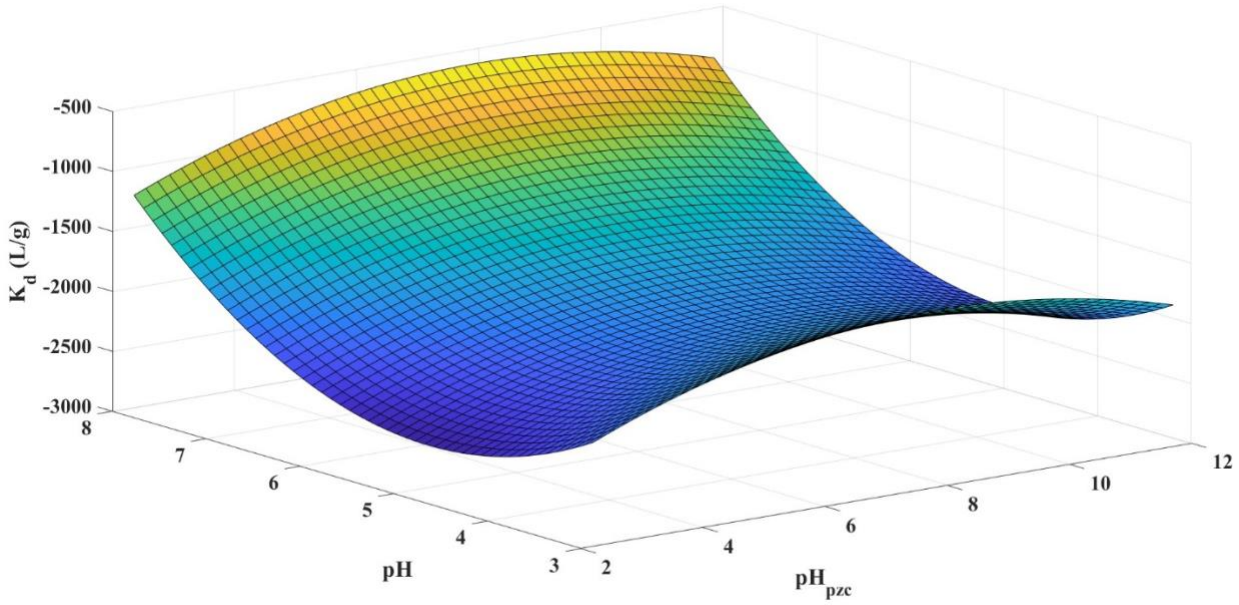


Figure 9: Response Surface plot showing the combined effect of pH and $pH_{pzc}$ on $K_d$.

These findings emphasize the critical role of pH control in PFAS adsorption and suggest that selecting adsorbents with a high $pH_{pzc}$ enhances removal efficiency, particularly under neutral to slightly acidic conditions. The significant p-values confirm that both pH and $pH_{pzc}$ should be considered key design parameters in optimizing adsorption materials for PFAS remediation.

### 3.4 Feature Importance

Below is an example of how one might interpret and discuss the feature-importance results for the three models (Random Forest, Gradient Boost, and XGBoost) in the context of predicting the PFAS distribution coefficient ($K_d$) and adsorption behavior. The values shown are the raw "importance" outputs from each algorithm rather than normalized scores, so direct comparisons within a single model are typically more meaningful than across models. Nevertheless, looking at all three can provide insights into which variables tend to be more (or less) influential overall.

As shown in Figure 10, for the Random Forest model, surface area (176354.9), Initial Concentration (145460.2), and $pH_{pzc}$ (114315.3) have notably large importance scores. Surface Area often correlates strongly with adsorption capacity; a larger surface area typically enhances the adsorbent's ability to bind PFAS. Initial Concentration can drive adsorption kinetics and

equilibrium partitioning—higher initial PFAS levels can lead to greater sorption until saturation is approached. $pH_{pzc}$ determines the surface charge of many adsorbents; being high here suggests that shifts in surface charge strongly affect PFAS attraction or repulsion.

$pK_a$ (12889.1), Molecular Weight (9937.0), and Log $K_{ow}$ (9432.5) fall into a middle-tier importance. $pK_a$ reflects the acidity of PFAS, influencing the ionization state. Molecular Weight (size of the PFAS compound) may affect diffusion and pore accessibility. Log $K_{ow}$ captures hydrophobicity and partially predicts how a PFAS might partition onto the solid media versus water.

pH (6058.0), E (5381.7), S (5285.3), and Dose (4918.7) occupy a somewhat lower tier but remain non-trivial. The solution pH can affect PFAS ionization and adsorbent surface charge. Dose (g/L) likely matters because the mass of available adsorbent alters the total removal capacity. E and S (possibly parameters describing molecular structure or solvation) show moderate importance, suggesting a partial influence on adsorption.

B (3676.8), A (3269.5), V (2567.8), and Temperature (229.3) have the smallest importance in Random Forest. While these features appear less critical, even lower-ranked variables can still modulate $K_d$ under certain conditions. Overall, Random Forest strongly underscores surface area, initial concentration, and $pH_{pzc}$ as top factors in determining PFAS adsorption and distribution.

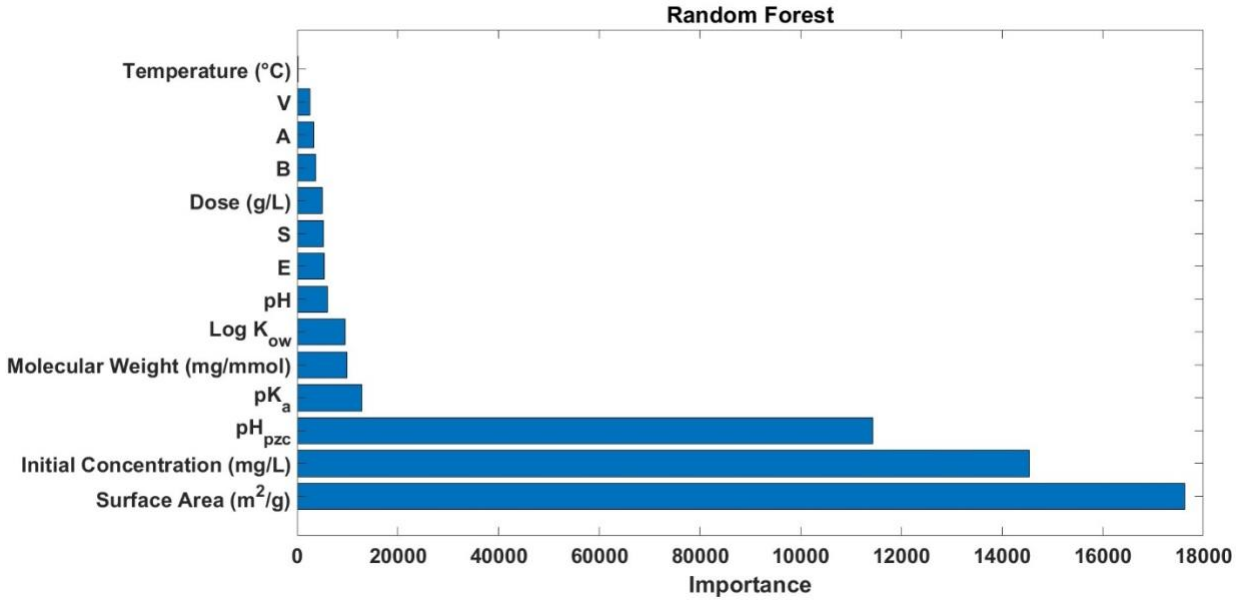


Figure 10: Feature importance plot for Random Forest model.

Initial Concentration (13445.3) and Surface Area (6789.7) dominate the importance in the Gradient Boost model as shown in Figure 11. Consistent with Random Forest, the amount of PFAS initially present and the available surface area of the adsorbent are the largest drivers of the predicted $K_d$.

Log $K_{ow}$ (19.1), $pH_{pzc}$ (10.5), $pK_a$, and Molecular Weight (8.7) form a secondary importance cluster. This again indicates that hydrophobicity (Log $K_{ow}$), ionization tendencies ($pH_{pzc}$, $pK_a$), and molecular size all play a role—albeit less crucial than surface area or initial concentration.

Dose (g/L) (7.3), Temperature (5.6), pH (4.7), and S (4.6) follow, showing moderate influence. Notably, the solution pH remains relevant but at a smaller magnitude than in the Random Forest result.

V (1.5), E (0.2), and especially A (0.0), B (0.0) contributed minimally or not at all in Gradient Boost splits. A zero importance often indicates those variables were never used in the boosted decision trees (or used so little that they did not improve predictive performance). Thus, Gradient Boost findings align generally with Random Forest: Initial Concentration and Surface Area stand out as top features, with some moderate roles for Log $K_{ow}$, $pH_{pzc}$, $pK_a$, and Molecular Weight.

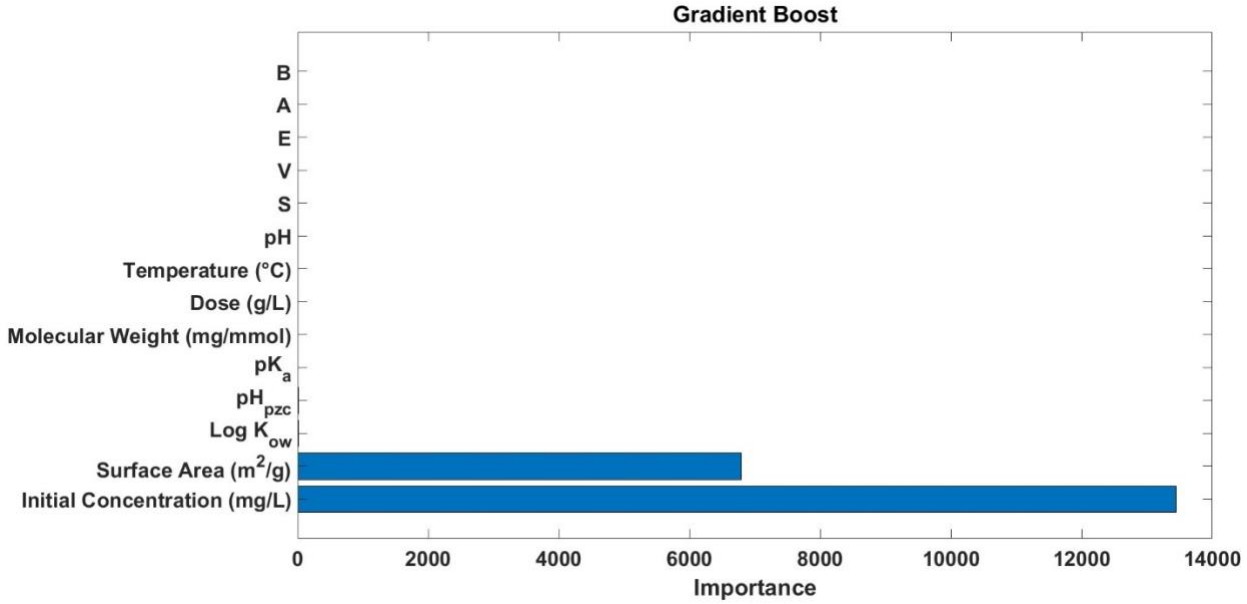


Figure 11: Feature importance plot for Gradient Boost model.

For the XGB model, as shown in Figure 12, Initial Concentration (71252.3) and Surface Area (33399.1) are again the top factors by a large margin. This reaffirms the strong dependence of $K_d$ on the dose of PFAS present in solution initially and the available sorption area.

$pH_{pzc}$ (44.2) appears as the third-highest influencer, followed by pH (23.6) and Dose (15.2). This suggests that in XGB's trees, surface charge conditions and the solution pH remain quite important for adsorption behavior.

Temperature (11.3), Log $K_{ow}$ (11.1), $pK_a$ (10.9), S (8.3), and Molecular Weight (5.1) cluster at moderate levels. V (1.3) again has low influence, and A (0.0), B (0.0), and E (0.0) do not contribute measurably to improving model performance.

Hence, XGB also confirms the overarching trend that Initial Concentration and Surface Area are pivotal to predicting $K_d$, with $pH_{pzc}$, pH, and other chemical descriptors playing smaller but non-negligible roles.

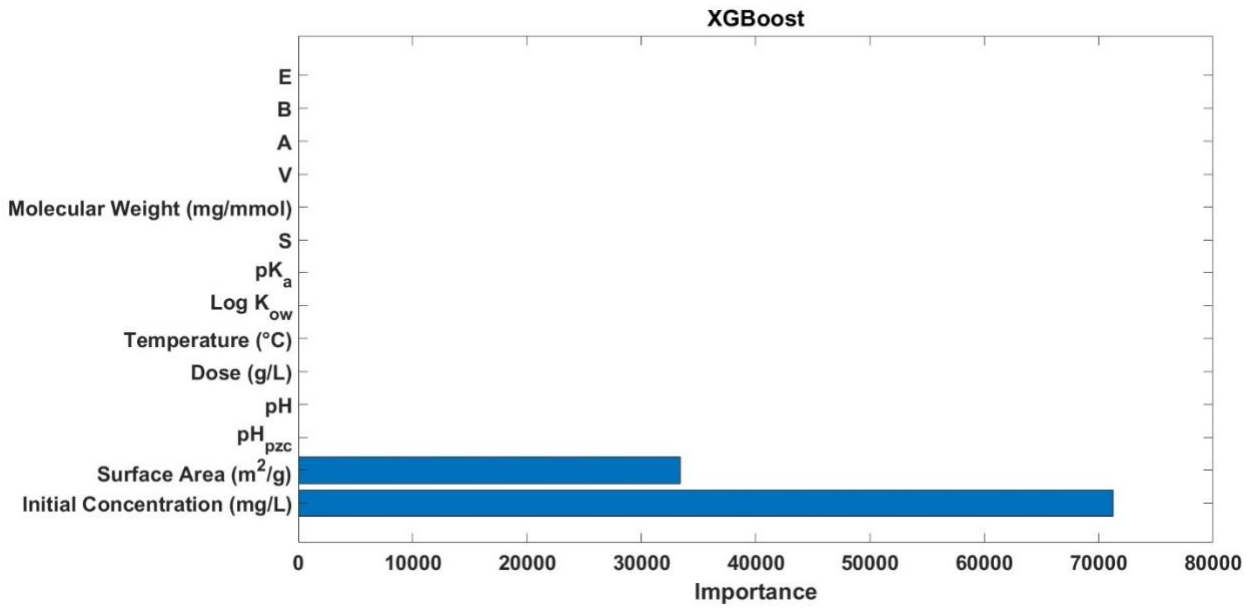


Figure 12: Feature importance plot for Extreme Gradient Boost (XGB) model.

All three methods (RF, GB, XGB) highlight Surface Area and Initial PFAS Concentration as top predictors. In practice, this aligns well with adsorption science: a larger surface area provides more active sites for PFAS attachment, and the initial PFAS loading drives sorption kinetics, potentially impacting mass transfer and equilibrium capacity.

$pH_{pzc}$ and pH are also significant, especially in Random Forest, implying that surface charge conditions strongly influence PFAS binding. Molecular descriptors like $pK_a$, Log $K_{ow}$, and Molecular Weight provide mid-range importance, indicating that hydrophobicity, ionization, and molecular size can further modulate adsorption.

Other variables such as Dose, Temperature, S, and E provide lower-tier effects, and some features (A, B, E) show zero importance under certain boosting algorithms. All three algorithms converge on the conclusion that the Surface Area of the adsorbent and the Initial Concentration of PFAS in solution are critical factors shaping the distribution coefficient ($K_d$). Variables tied to surface chemistry ($pH_{pzc}$) and PFAS properties ($pK_a$, Log $K_{ow}$, molecular weight) further refine predictions by capturing how electrostatics, hydrophobicity, and size modulate adsorption behavior.

## 4 Conclusion

1) Hybrid RSM-ML models significantly improved PFAS adsorption prediction accuracy, with the Meta HOP-RSM-GB model achieving near-perfect performance ($R^2$ = 1.00, RMSE = 10.59, MSE = 112.21, MAE = 3.95), outperforming both standalone RSM and machine learning models. This demonstrated the power of combining statistical and ML-driven techniques in adsorption modeling.
2) Surface area and hydrophobicity (log $K_{ow}$) were identified as dominant factors influencing PFAS adsorption, with higher log $K_{ow}$ values correlating with greater $K_d$ regardless of

surface area. This highlighted the importance of PFAS physicochemical properties in determining adsorption efficiency.

3) Electrostatic interactions, governed by pH and $pH_{pzc}$, played a critical role in adsorption efficiency. Adsorption was enhanced at low pH and high $pH_{pzc}$ due to stronger electrostatic attraction, while high pH led to significant desorption, reinforcing the need for pH control in remediation strategies.
4) Response surface analysis revealed significant non-linear interactions between adsorption parameters, indicating that one-variable-at-a-time (OFAT) approaches are insufficient for optimizing PFAS removal. Instead, data-driven modeling is essential for capturing complex adsorption behaviors in a multiparameter process.
5) Hybrid models, particularly RMSE-based and meta-model approaches, provided the most accurate predictions of $K_d$ by effectively integrating polynomial regression with ensemble learning. This highlighted the value of machine learning in addressing the limitations of traditional statistical modeling in adsorption studies.
6) Higher-order polynomial (HOP-RSM) regression alone exhibited poor predictive performance ($R^2 = 0.04$), underscoring the necessity of hybrid approaches to accurately model PFAS adsorption across a wide range of conditions.
7) Surface plots confirmed that adsorption optimization required balancing adsorbent surface chemistry and operational conditions, with the highest $K_d$ values observed at moderate surface areas (1000 – 1500 $m^2/g$), $pH_{pzc}$ values (6 – 10), and temperatures (30 – 35 °C).
8) Machine learning hybridization with RSM can significantly reduce the number of experiments required for process optimization, offering a scalable approach for accelerating PFAS remediation research and minimizing experimental costs.
9) This study established hybrid RSM-ML modeling as a powerful framework for optimizing PFAS adsorption, providing a pathway for improved adsorbent design, predictive adsorption modeling, and data-driven decision-making in environmental remediation efforts.
**10)** Surface Area and Initial Concentration consistently emerge as the most influential features in determining the PFAS distribution coefficient ($K_d$), while $pH_{pzc}$, pH, and molecular descriptors ($pK_a$, Log $K_{ow}$, Molecular Weight) provide additional insights into adsorption behavior. Across all three algorithms — Random Forest, Gradient Boost, and Extreme Gradient Boost—the data underscore that both adsorbent surface chemistry and PFAS properties significantly modulate $K_d$ values.

## References


Abraham, M. H., & Walsh, D. P. (1992). Hydrogen bonding: XXIII. Application of the new solvation equation to log Vg values for solutes on carbonaceous adsorbents. *Journal of Chromatography A*, *627*(1), 294–299. https://doi.org/10.1016/0021-9673(92)87210-Y

Ateia, M., Attia, M. F., Maroli, A., Tharayil, N., Alexis, F., Whitehead, D. C., & Karanfil, T. (2018). Rapid Removal of Poly- and Perfluorinated Alkyl Substances by Poly(ethylenimine)-Functionalized Cellulose Microcrystals at Environmentally Relevant Conditions. *Environmental Science & Technology Letters*, *5*(12), 764–769. https://doi.org/10.1021/acs.estlett.8b00556

Burg, P., Abraham, M. H., & Cagniant, D. (2003). Methods of determining polar and non-polar sites on carbonaceous adsorbents. The contribution of the linear solvation energy relationship approach. *Carbon*, *41*(5), 867–879. https://doi.org/10.1016/S0008-6223(03)00018-6

Campos-Pereira, H., Kleja, D. B., Sjöstedt, C., Ahrens, L., Klysubun, W., & Gustafsson, J. P. (2020). The Adsorption of Per- and Polyfluoroalkyl Substances (PFASs) onto Ferrihydrite Is Governed by Surface Charge. *Environmental Science & Technology*, *54*(24), 15722–15730. https://doi.org/10.1021/acs.est.0c01646

Chang, P.-H., Jiang, W.-T., & Li, Z. (2019). Removal of perfluorooctanoic acid from water using calcined hydrotalcite – A mechanistic study. *Journal of Hazardous Materials*, *368*, 487–495. https://doi.org/10.1016/j.jhazmat.2019.01.084

Chang, P.-H., Li, Z., & Jiang, W.-T. (2020). Calcination of hydrotalcite to enhance the removal of perfluorooctane sulfonate from water. *Applied Clay Science*, *190*, 105563. https://doi.org/10.1016/j.clay.2020.105563

Chen, W., Zhang, X., Mamadiev, M., & Wang, Z. (2017). Sorption of perfluorooctane sulfonate and perfluorooctanoate on polyacrylonitrile fiber-derived activated carbon fibers: In comparison with activated carbon. *RSC Advances*, *7*(2), 927–938. https://doi.org/10.1039/C6RA25230C

Chen, X., Xia, X., Wang, X., Qiao, J., & Chen, H. (2011a). A comparative study on sorption of perfluorooctane sulfonate (PFOS) by chars, ash and carbon nanotubes. *Chemosphere*, *83*(10), 1313–1319. https://doi.org/10.1016/j.chemosphere.2011.04.018

Chen, X., Xia, X., Wang, X., Qiao, J., & Chen, H. (2011b). A comparative study on sorption of perfluorooctane sulfonate (PFOS) by chars, ash and carbon nanotubes. *Chemosphere*, *83*(10), 1313–1319. https://doi.org/10.1016/j.chemosphere.2011.04.018

de S. Furtado, R. X., Sabatini, C. A., Zaiat, M., & Azevedo, E. B. (2021). Perfluorooctane sulfonic acid (PFOS) degradation by optimized heterogeneous photocatalysis (TiO2/UV) using the response surface methodology (RSM). *Journal of Water Process Engineering*, *41*, 101986. https://doi.org/10.1016/j.jwpe.2021.101986

Deng, S., Zhang, Q., Nie, Y., Wei, H., Wang, B., Huang, J., Yu, G., & Xing, B. (2012). Sorption mechanisms of perfluorinated compounds on carbon nanotubes. *Environmental Pollution*, *168*, 138–144. https://doi.org/10.1016/j.envpol.2012.03.048

Fagbayigbo, B. O., Opeolu, B. O., Fatoki, O. S., Akenga, T. A., & Olatunji, O. S. (2017). Removal of PFOA and PFOS from aqueous solutions using activated carbon produced from Vitis vinifera leaf litter. *Environmental Science and Pollution Research*, *24*(14), 13107–13120. https://doi.org/10.1007/s11356-017-8912-x

Jian, J.-M., Zhang, C., Wang, F., Lu, X., Wang, F., & Zeng, E. Y. (2019). Effect of solution chemistry and aggregation on adsorption of perfluorooctanesulphonate (PFOS) to nano-sized alumina. *Environmental Pollution*, *251*, 425–433. https://doi.org/10.1016/j.envpol.2019.05.025

Kamlet, M. J., Doherty, R. M., Abraham, M. H., & Taft, R. W. (1985). Linear solvation energy relationships. 33. An analysis of the factors that influence adsorption of organic compounds on activated carbon. *Carbon*, *23*(5), 549–554. https://doi.org/10.1016/0008-6223(85)90091-0

Karbassiyazdi, E., Fattahi, F., Yousefi, N., Tahmassebi, A., Taromi, A. A., Manzari, J. Z., Gandomi, A. H., Altaee, A., & Razmjou, A. (2022). XGBoost model as an efficient machine learning approach for PFAS removal: Effects of material characteristics and operation conditions. *Environmental Research*, *215*, 114286. https://doi.org/10.1016/j.envres.2022.114286

Lei, X., Lian, Q., Zhang, X., Wang, T., Gee, M., Holmes, W., Jin, S., Ponnusamy, S. K., Gang, D. D., & Zappi, M. E. (2022). Removal of perfluorooctanoic acid via polyethyleneimine modified graphene oxide: Effects of water matrices and understanding mechanisms. *Chemosphere*, *308*, 136379. https://doi.org/10.1016/j.chemosphere.2022.136379

Lei, X., Yao, L., Lian, Q., Zhang, X., Wang, T., Holmes, W., Ding, G., Gang, D. D., & Zappi, M. E. (2022). Enhanced adsorption of perfluorooctanoate (PFOA) onto low oxygen content ordered mesoporous carbon (OMC): Adsorption behaviors and mechanisms. *Journal of Hazardous Materials*, *421*, 126810. https://doi.org/10.1016/j.jhazmat.2021.126810

Liu, L., Li, D., Li, C., Ji, R., & Tian, X. (2018). Metal nanoparticles by doping carbon nanotubes improved the sorption of perfluorooctanoic acid. *Journal of Hazardous Materials*, *351*, 206–214. https://doi.org/10.1016/j.jhazmat.2018.03.001

Liu, T., Gu, Y., Xing, D. Y., Dong, W., & Wu, X. (2018). Rapid and high-capacity adsorption of PFOS and PFOA by regenerable ammoniated magnetic particle. *Environmental Science and Pollution Research*, *25*(14), 13813–13822. https://doi.org/10.1007/s11356-018-1578-1

McNamara, J. D., Franco, R., Mimna, R., & Zappa, L. (2018). Comparison of Activated Carbons for Removal of Perfluorinated Compounds From Drinking Water. *Journal - American Water Works Association*, *110*(1), E2–E14. https://doi.org/10.5942/jawwa.2018.110.0003

Meng, P., Fang, X., Maimaiti, A., Yu, G., & Deng, S. (2019). Efficient removal of perfluorinated compounds from water using a regenerable magnetic activated carbon. *Chemosphere*, *224*, 187–194. https://doi.org/10.1016/j.chemosphere.2019.02.132

Naim Shaikh, M. A., & Nawaz, T. (2024). Highly Efficient Cationic Surfactant Functionalized Alginate Hydrogel for Perfluorooctanoic Acid Adsorption: Optimization through Response Surface Methodology and Performance Evaluation for Aqueous Media. *ACS ES&T Water*, *4*(7), 3078–3088. https://doi.org/10.1021/acsestwater.4c00319

Patel, H. V., Greer, M., Brazil, B., Yu, W., Hamoush, S., Zhang, L., & Zhao, R. (2025). Adsorption capacity and mechanism of modified coal fly ash (CFA) for per- and polyfluoroalkyl substances (PFAS) in landfill leachate. *Journal of Hazardous Materials*, *484*, 136763. https://doi.org/10.1016/j.jhazmat.2024.136763

Pramanik, B. K., Pramanik, S. K., & Suja, F. (2015). A comparative study of coagulation, granular- and powdered-activated carbon for the removal of perfluorooctane sulfonate and perfluorooctanoate in drinking water treatment. *Environmental Technology*, *36*(20), 2610–2617. https://doi.org/10.1080/09593330.2015.1040079

673 Qian, J., Shen, M., Wang, P., Wang, C., Li, K., Liu, J., Lu, B., & Tian, X. (2017). Perfluorooctane
674 sulfonate adsorption on powder activated carbon: Effect of phosphate (P) competition,
675 pH, and temperature. *Chemosphere*, *182*, 215–222.
676 https://doi.org/10.1016/j.chemosphere.2017.05.033
677 Ross, I., McDonough, J., Miles, J., Storch, P., Thelakkat Kochunarayanan, P., Kalve, E., Hurst,
678 J., S. Dasgupta, S., & Burdick, J. (2018). A review of emerging technologies for
679 remediation of PFASs. *Remediation Journal*, *28*(2), 101–126.
680 https://doi.org/10.1002/rem.21553
681 Rostvall, A., Zhang, W., Dürig, W., Renman, G., Wiberg, K., Ahrens, L., & Gago-Ferrero, P.
682 (2018). Removal of pharmaceuticals, perfluoroalkyl substances and other micropollutants
683 from wastewater using lignite, Xylit, sand, granular activated carbon (GAC) and
684 GAC+Polonite ® in column tests – Role of physicochemical properties. *Water Research*,
685 *137*, 97–106. https://doi.org/10.1016/j.watres.2018.03.008
686 Senevirathna, S. T. M. L. D., Tanaka, S., Fujii, S., Kunacheva, C., Harada, H., Shivakoti, B. R.,
687 & Okamoto, R. (2010). A comparative study of adsorption of perfluorooctane sulfonate
688 (PFOS) onto granular activated carbon, ion-exchange polymers and non-ion-exchange
689 polymers. *Chemosphere*, *80*(6), 647–651.
690 https://doi.org/10.1016/j.chemosphere.2010.04.053
691 Sinha, S., Yang, C., Wu, E., & Acree, W. E. (2022). Abraham Solvation Parameter Model:
692 Examination of Possible Intramolecular Hydrogen-Bonding Using Calculated Solute
693 Descriptors. *Liquids*, *2*(3), Article 3. https://doi.org/10.3390/liquids2030009
694 Sprunger, L., Proctor, A., Acree, W. E., & Abraham, M. H. (2007). Characterization of the
695 sorption of gaseous and organic solutes onto polydimethyl siloxane solid-phase
696 microextraction surfaces using the Abraham model. *Journal of Chromatography A*,
697 *1175*(2), 162–173. https://doi.org/10.1016/j.chroma.2007.10.058
698 Tang, C. Y., Shiang Fu, Q., Gao, D., Criddle, C. S., & Leckie, J. O. (2010). Effect of solution
699 chemistry on the adsorption of perfluorooctane sulfonate onto mineral surfaces. *Water*
700 *Research*, *44*(8), 2654–2662. https://doi.org/10.1016/j.watres.2010.01.038
701 US EPA, O. (2024, April 10). *Per- and Polyfluoroalkyl Substances (PFAS)* [Reports and
702 Assessments]. https://www.epa.gov/sdwa/and-polyfluoroalkyl-substances-pfas
703 Wang, B., Lee, L. S., Wei, C., Fu, H., Zheng, S., Xu, Z., & Zhu, D. (2016). Covalent triazine-
704 based framework: A promising adsorbent for removal of perfluoroalkyl acids from
705 aqueous solution. *Environmental Pollution*, *216*, 884–892.
706 https://doi.org/10.1016/j.envpol.2016.06.062
707 Wang, F., Liu, C., & Shih, K. (2012). Adsorption behavior of perfluorooctanesulfonate (PFOS)
708 and perfluorooctanoate (PFOA) on boehmite. *Chemosphere*, *89*(8), 1009–1014.
709 https://doi.org/10.1016/j.chemosphere.2012.06.071
710 Wang, F., & Shih, K. (2011). Adsorption of perfluorooctanesulfonate (PFOS) and
711 perfluorooctanoate (PFOA) on alumina: Influence of solution pH and cations. *Water*
712 *Research*, *45*(9), 2925–2930. https://doi.org/10.1016/j.watres.2011.03.007
713 Xing, D. Y., Chen, Y., Zhu, J., & Liu, T. (2020). Fabrication of hydrolytically stable magnetic
714 core-shell aminosilane nanocomposite for the adsorption of PFOS and PFOA.
715 *Chemosphere*, *251*, 126384. https://doi.org/10.1016/j.chemosphere.2020.126384
716 Yang, A., Ching, C., Easler, M., Helbling, D. E., & Dichtel, W. R. (2020). Cyclodextrin Polymers
717 with Nitrogen-Containing Tripodal Crosslinkers for Efficient PFAS Adsorption. *ACS*
718 *Materials Letters*, *2*(9), 1240–1245. https://doi.org/10.1021/acsmaterialslett.0c00240

Yang, H., Kang, J.-K., Jeong, S., Park, S.-J., & Lee, C.-G. (2022). Removal of perfluorooctanoic acid from water using peroxydisulfate/layered double hydroxide system: Optimization using response surface methodology and artificial neural network. *Process Safety and Environmental Protection*, *167*, 368–377. https://doi.org/10.1016/j.psep.2022.09.032

Yoon, S., Park, J., Police, A. K. R., Choe, J. K., & Bae, S. (2025). Enhanced removal of perfluorooctanoic acid by aluminum-based metal–organic frameworks prepared by bauxite residue. *Journal of Hazardous Materials*, *483*, 136687. https://doi.org/10.1016/j.jhazmat.2024.136687

Yu, Q., Zhang, R., Deng, S., Huang, J., & Yu, G. (2009). Sorption of perfluorooctane sulfonate and perfluorooctanoate on activated carbons and resin: Kinetic and isotherm study. *Water Research*, *43*(4), 1150–1158. https://doi.org/10.1016/j.watres.2008.12.001

Zhang, D., Luo, Q., Gao, B., Chiang, S.-Y. D., Woodward, D., & Huang, Q. (2016a). Sorption of perfluorooctanoic acid, perfluorooctane sulfonate and perfluoroheptanoic acid on granular activated carbon. *Chemosphere*, *144*, 2336–2342. https://doi.org/10.1016/j.chemosphere.2015.10.124

Zhang, D., Luo, Q., Gao, B., Chiang, S.-Y. D., Woodward, D., & Huang, Q. (2016b). Sorption of perfluorooctanoic acid, perfluorooctane sulfonate and perfluoroheptanoic acid on granular activated carbon. *Chemosphere*, *144*, 2336–2342. https://doi.org/10.1016/j.chemosphere.2015.10.124

Zhang, K., Zhong, S., & Zhang, H. (2020). Predicting Aqueous Adsorption of Organic Compounds onto Biochars, Carbon Nanotubes, Granular Activated Carbons, and Resins with Machine Learning. *Environmental Science & Technology*, *54*(11), 7008–7018. https://doi.org/10.1021/acs.est.0c02526

Zhang, Q., Deng, S., Yu, G., & Huang, J. (2011). Removal of perfluorooctane sulfonate from aqueous solution by crosslinked chitosan beads: Sorption kinetics and uptake mechanism. *Bioresource Technology*, *102*(3), 2265–2271. https://doi.org/10.1016/j.biortech.2010.10.040

Zhao, L., Bian, J., Zhang, Y., Zhu, L., & Liu, Z. (2014). Comparison of the sorption behaviors and mechanisms of perfluorosulfonates and perfluorocarboxylic acids on three kinds of clay minerals. *Chemosphere*, *114*, 51–58. https://doi.org/10.1016/j.chemosphere.2014.03.098

Zhi, Y., & Liu, J. (2016). Surface modification of activated carbon for enhanced adsorption of perfluoroalkyl acids from aqueous solutions. *Chemosphere*, *144*, 1224–1232. https://doi.org/10.1016/j.chemosphere.2015.09.097

Zhou, Q., Deng, S., Yu, Q., Zhang, Q., Yu, G., Huang, J., & He, H. (2010). Sorption of perfluorooctane sulfonate on organo-montmorillonites. *Chemosphere*, *78*(6), 688–694. https://doi.org/10.1016/j.chemosphere.2009.12.005